NASA CR-144775

FEBRUARY 1976

EXPERIMENT DEFINITION PHASE SHUTTLE LABORATORY

LDRL-10.6 EXPERIMENT

SIXTH QUARTERLY REPORT AND TWELFTH MONTHLY REPORT

NASA Contract NAS 5-20018

(NASA-CR-144775) EXPERIMENT DEFINITION PHASE SHUTTLE LABORATORY. LDRL-10.6 EXPERIMENT Quarterly Report, 27 Sept. 1975 - 26 Jan. 1976 (Hughes Aircraft Co.) 34 p HC $4.00 CSCL 14E G3/14

N76-27305

Unclas 44490

HUGHES

HUGHES AIRCRAFT COMPANY
SPACE AND COMMUNICATIONS GROUP

Hughes Ref No. D0824 SCG 60997R

FEBRUARY 1976

EXPERIMENT DEFINITION PHASE SHUTTLE LABORATORY

LDRL-10.6 EXPERIMENT

•

SIXTH QUARTERLY REPORT
AND
TWELFTH MONTHLY REPORT

NASA Contract NAS 5-20018

HUGHES

HUGHES AIRCRAFT COMPANY
SPACE AND COMMUNICATIONS GROUP

Hughes Ref No. D0824 SCG 60097R

CONTENTS

1. INTRODUCTION

This report for the Experiment Definition Phase of the Shuttle Laboratory LDRL 10.6 Micrometer Experiment (Contract NAS 5-20018) covers the period from 27 September 1975 through 26 January 1976. It combines the sixth quarterly report with the twelfth monthly report. A large portion of the hardware being manufactured for the program was completed during the early portion of the month of January, so the quarterly report has been delayed to allow photographs and other data to be included. (The monthly report format precludes photo reproduction.)

Activities during the report period included:

Optomechanical Subsystem

- Completion of detail drawings
- Completion of the beryllium subassembly
- Fabrication, checking, and weighing of approximately 95 percent of the detailed parts
- Dry film lubrication of the bearings and gears
- Initiation of assembly of the gimbals

Optics

- Update of the detailed optical layout
- Receipt of nine mirrors and the pre-expander

Miscellaneous

- Delivery of draft material for the final report
- Completion of optical testing of the 10.6 μm receiver
- Receipt, assembly, and checkout of NASA test console

2. OPTOMECHANICAL SUBSYSTEM

Detailing of the optomechanical structure including the beryllium housing, gimbals, optical mounts, image motor compensator mounts and related parts has been completed and fabrication of all parts has begun. About 95 percent of the pieces have been finished. Table 1 is a list of all detail drawings by item number, drawing number, and part name. Parts that have been completed have been weighed; these weights are also listed in Table 1. Many of the parts for the mechanical structure have been fabricated from aluminum or steel in the interest of economy, and this detailed listing of weights will provide an accurate estimate of possible weight savings in any future modification program.

A fixture to aid the assembly and disassembly of the gimbal bearings (132-1/8 inch diameter balls in each bearing) has been fabricated. All bearings and gears have been disassembled, dry-film-lubricated by sputter coating with moly-disulfide, and reassembled.

All purchased items including the motors from Inland Corporation, techometers and resolvers from Singer Corporation, and optical encoders have been received. Assembly of these parts to form the gimbal structures has begun.

Figure 1 is a photograph of the beryllium housing for the optomechanical subsystem. Visible in the picture is the mounting interface for the outer gimbal located at one end of the structure and the opening in the side where the inner gimbal is attached. The entire structure is reinforced with angle gussets, one of which is visible inside the box. All gussets and side panels are beryllium; the end pieces are steel. In this view the top plate unbolts to provide easy access to the internal mounts for the optics.

Figure 2 is a photo of the parts that comprise one of the gimbal structures and also contains the parts for the secondary mirror mount and folding diagonal (optical elements 4 and 5). The perforated ring in the top right of the picture is the large drive gear for the tachometer, resolver, and optical encoder. Immediately below this gear are the smaller gears and shafts for driving these components. The element at the bottom right of the picture is the large diameter motor with the brush block located bottom center. The remaining large diameter parts form the stator and rotor of the gimbal together with a spacer and preload spring.

TABLE 1. LIST OF PARTS AND ACTUAL WEIGHTS

Item	Part Number	Part Name	Weight, lbs	Quantity	Total
2	3484002		0.443	1	0.443
	3484002-99				
	3484002-98				
	3484002-97				
	3484002-96				
	3484002-95				
	3484002-94		≈ 3.25	1	3.25
	3484002-93				
	3484002-92				
	3484002-91				
	3484002-90				
	3484002-89		4.988	1	4.988
	3484002-88		2.510	1	2.510
	3484002-87				
	3484002-86				
	3484002-85				
3	3484003	Housing, gimbal	4.488	2	8.976
5	3484005-1	Shaft, gimbal	4.225	1	4.225
5	3484005-2	Shaft, gimbal	1.810	1	1,810
6	3484007	Ring, primary mirrors	0.306	1	0.306
7	3484008	Support, F-mirrors sm	0.603	1	0.603
8	3484009	Ring, clamp	0.220	1	0.220
9	3484010	Support, mirrors	0.044	1	0.044
10	3484011	Bracket, support	0.785	1	0.785
11	3484012	Mount, mirrors			
12	3484013	Ring, house, attachment			
4	3484004	Gear, assembly			
13	3484017	Bracket, gear support	0.800	2	0.800
29	3484061	Spac, gear resolver	0.023	2	0.023
30	3484062	Spac, gear tach	0.032	2	0.032
23	3484027-1,-2	Gear, tach drive	0.019	2	0.019
22	3484026	Gear, resolver	0.162	2	0.162
21	3484025-1,-2,-3	Gear, shaft, drive	0.210	2	0.210
14	3484018	Shaft, gear	0.088	2	0.088
15	3484019	Spring, preload	0.907	2	0.907
18	3484022	Clamp, point mirror			
16	3484020	Ring, housing, point			
17	3484021	Housing, point mirror			
19	3484023	Ring, secondary mirrors	0.018	1	0.018

Table 1 (Continued)

Item	Part Number	Part Name	Weight, lbs	Quantity	Total
20	3484024	Gear, drive	2.301	2	2.301
24	3484028	Clamp, ring	0.31	1	0.31
25	3484029	Plate, mirror mounting			
26	3484030	Plate, IMC mounting	0.682	1	0.682
27	3484031	Bracket, switch mounting			
28	3484034	Shim, preload (1/2)			
31	3484063	Ring, inner			
32	3484064	Cover, gear			
33	3484065	Blk, zero position lock	0.144	2	0.144
34	3484066	Support, positioner pin	0.265	2	0.265
35	3484067	Plate, IMC stop	0.083		0.083
36	3484068	Relay, mirror support			
37		Pre-expander support			
		LDR support			
38	3484006	Bearing, support	0.582	2	0.582
		Encoder	0.843	2	0.843
		Resolver	0.497	2	0.497
		Tach	0.532	2	0.532
		Torquer – Coil			
		Torquer – Brush	0.347	2	0.347
		Switch	0.047	2	0.047
		Total (less mirrors and miscellaneous hardware)			36.37

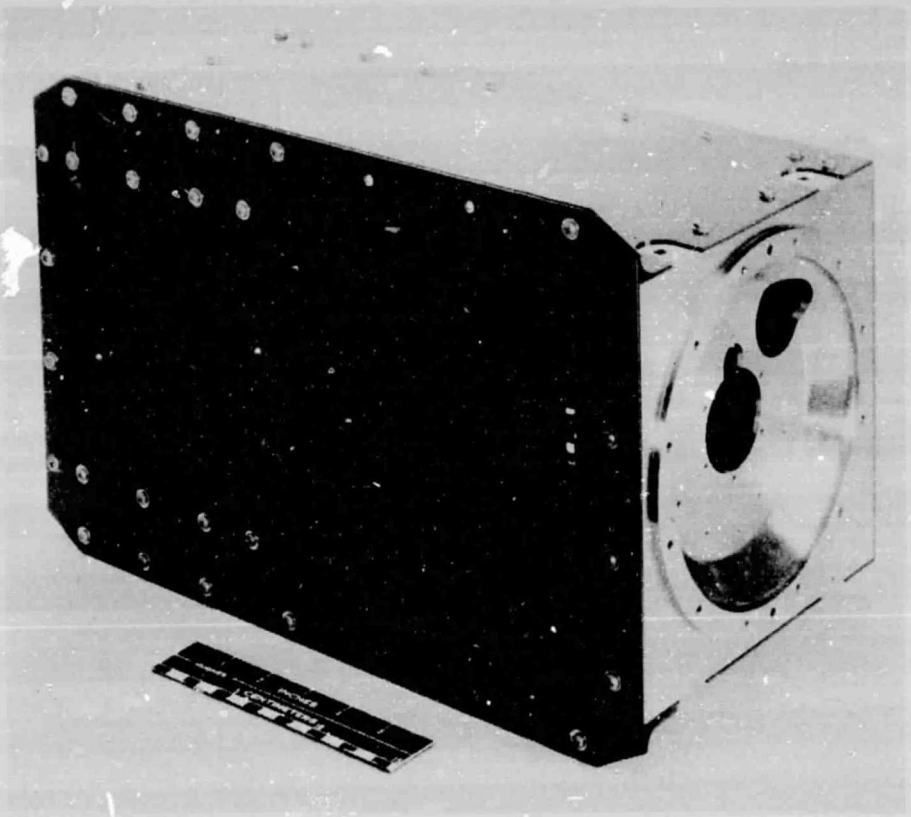

FIGURE 1. BERYLLIUM OPTOMECHANICAL STRUCTURE (PHOTO 4C00636)

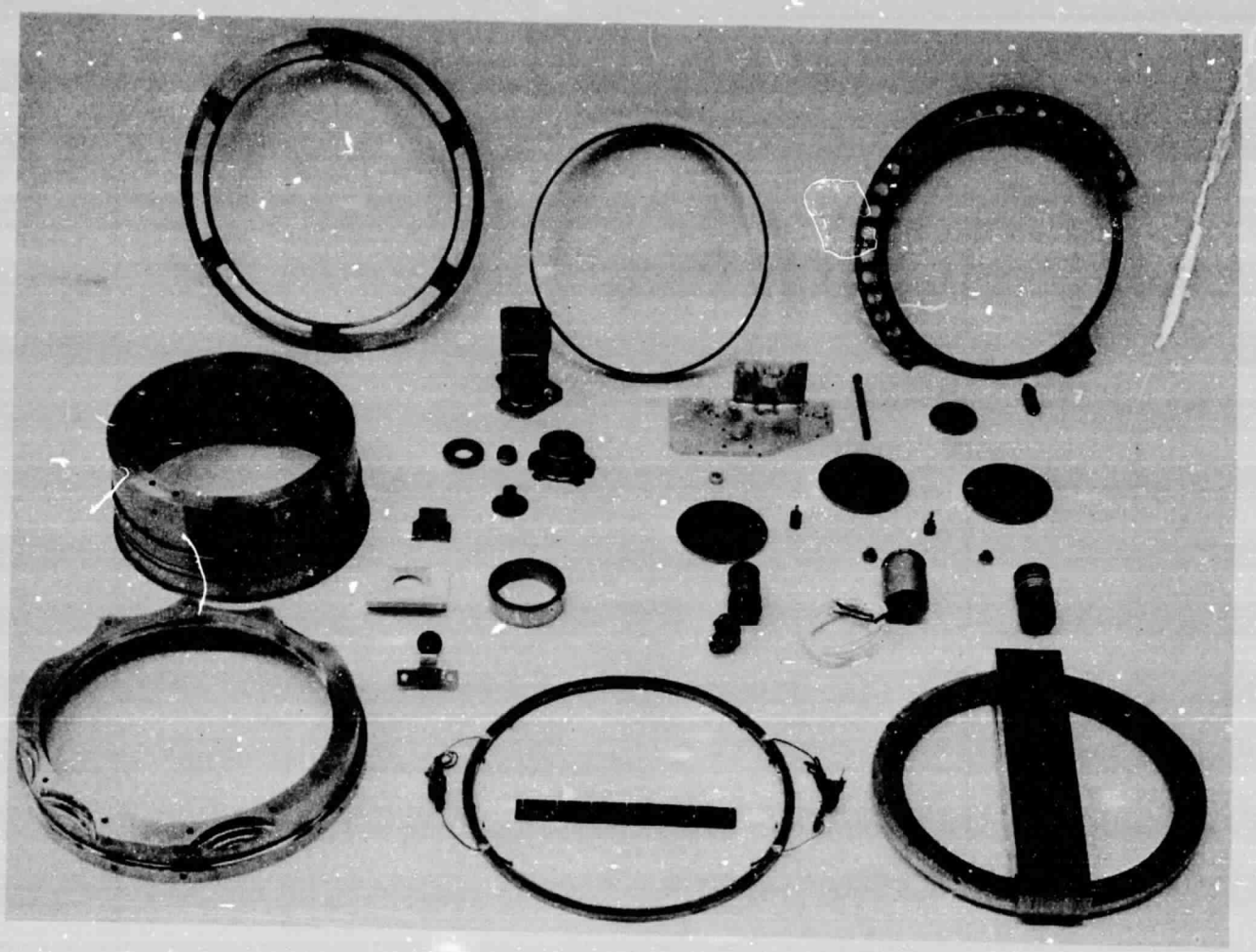

FIGURE 2. GIMBAL PARTS AND SECONDARY MIRROR MOUNT (PHOTO 4R43318)

3. OPTICS

A new optical layout incorporating the most recent changes in design has been generated and is shown in Figure 3. This drawing should be compared with the diagram published on page 97 of the third quarterly report for this program. Although many dimensions have been changed by small amounts, the most significant change is in the diameter of the opening in mirror 2. The reduction was made possible by the obscuration ratio change discussed in the fifth quarterly report and is responsible for many of the shifts in element spacing to prevent loss of signal due to vignetting.

All of the optical elements have been received. The pre-expander was delivered with a faulty folding mirror installed, but the vendor had warned Hughes of this problem and is currently fabricating a replacement mirror. The fault consists of excessive chipping around the small center hole in the mirror as well as some chipping around the larger holes. It is expected that the replacement mirror will be received near the end of February.

The mirror vendor (Applied Optics Center) conducted interferometric tests of all mirrors to confirm that all specifications have been met. These data are reproduced here to provide a permanent record of delivered mirror quality.

Figure 4 shows two interferograms of element 1, taken with a 12-inch interferometer and a 0.589 μm light source. The data sheet claims an overall deviation of 1 fringe, local smoothness of better than 1 arcsec, and astigmatism of 3/8 fringe, all measured over the clear aperture. Surface quality is better than 80/50.

Figure 5 shows two interferograms for element 2, the large folding mirror, taken under the same conditions as element 1. The data sheet for this mirror claims 1-1/4 fringes overall deviation, better than 1 arcsec local smoothness, and 1/4 fringe astigmatism. Surface quality is better than 60/40.

Figure 6 is the beryllium primary mirror interferogram. Measurements on this element were made using a HeNe laser 8-inch interferometer, operating at 0.633 μm. The pictures clearly show zones where the radius of curvature abruptly changes, although the changes are small. The disadvantage of this form of error is that it is systematic rather than random, but

OPTICAL CHARACTERISTICS OF PRE-EXPANDER	
MAGNIFICATION	6.046
F-NUMBER PRIMARY	4.17
F-NUMBER SECONDARY	4.17
FIELD OF VIEW	0°
DIAMETER OBSCURATION RATIO	.173
OUTPUT BEAM DIAMETER	2.54 CM (1.00 IN)

OPTICAL CHARACTERISTICS OF BEAM EXPANDER	
MAGNIFICATION	7.087
F-NUMBER PRIMARY	1.8
F-NUMBER SECONDARY	1.23 *
FIELD OF VIEW	±½°
DIAMETER OBSCURATION RATIO	.362
OUTPUT BEAM DIAMETER	18CM (7.0866 IN)

* EFFECTIVE F-NUMBER = 1.5

LIMIT RAY DATA		
SURFACE	LIMIT RAY	COMPONENT DRAWING
PRE-EXPANDER LARGE FOLD MIRROR ELEM X	.311 *	3482108
PRE-EXPANDER SECONDARY MIRROR ELEM XII	.220	3482107
PRE-EXPANDER PRIMARY MIRROR ELEM XI	1.270	3482106
PRE-EXPANDER LARGE FOLD MIRROR ELEM X	1.796 *	3482108
RELAY MIRROR ELEM IX	1.796 *	3482072
RELAY MIRROR ELEM VIII	1.796 *	3482072
IMC MIRROR ELEM VII	1.796 *	3482071
STOP	1.270	
IMC MIRROR ELEM VII	1.796 *	3482071
SMALL FOLDING MIRROR ELEM V	1.989 *	3482070
SECONDARY MIRROR ELEM IV	1.541	3482069
PRIMARY MIRROR ELEM III	9.000	3482068
LARGE FOLDING MIRROR ELEM II	13.113 *	3482067
POINTING MIRROR ELEM I	13.455 *	3482066

* MEASURED ALONG MIRROR SURFACE AT 45°

ALL DIMENSIONS ARE IN CENTIMETERS

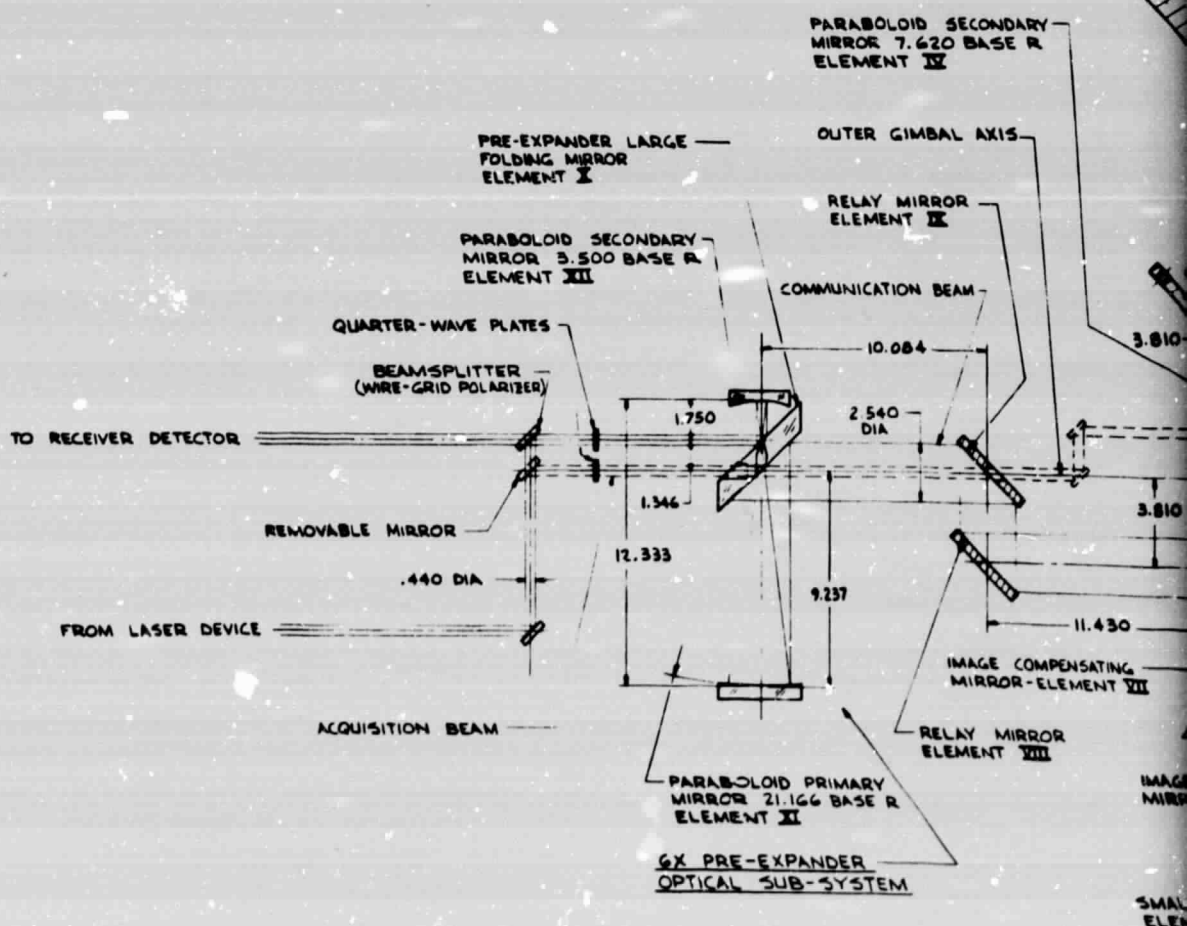

FIGURE 3. REVISED OPTICAL LAYOUT

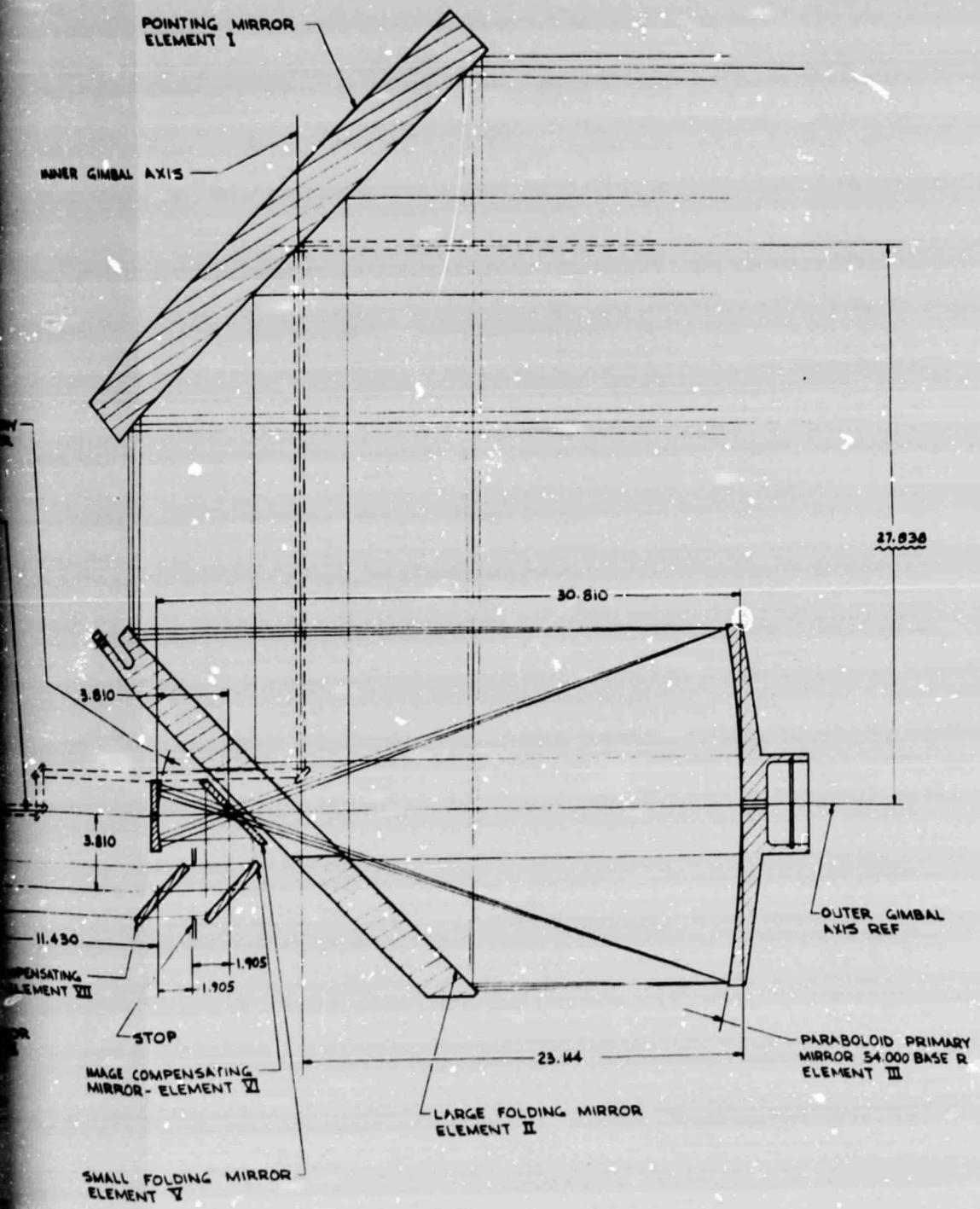
POINTING MIRROR
ELEMENT I
INNER GIMBAL AXIS
27.838
30.810
3.810
3.810
11.430
1.905
1.905
STOP
IMAGE COMPENSATING
MIRROR - ELEMENT VI
SMALL FOLDING MIRROR
ELEMENT V
23.144
LARGE FOLDING MIRROR
ELEMENT II
OUTER GIMBAL
AXIS REF
PARABOLOID PRIMARY
MIRROR 54.000 BASE R
ELEMENT III

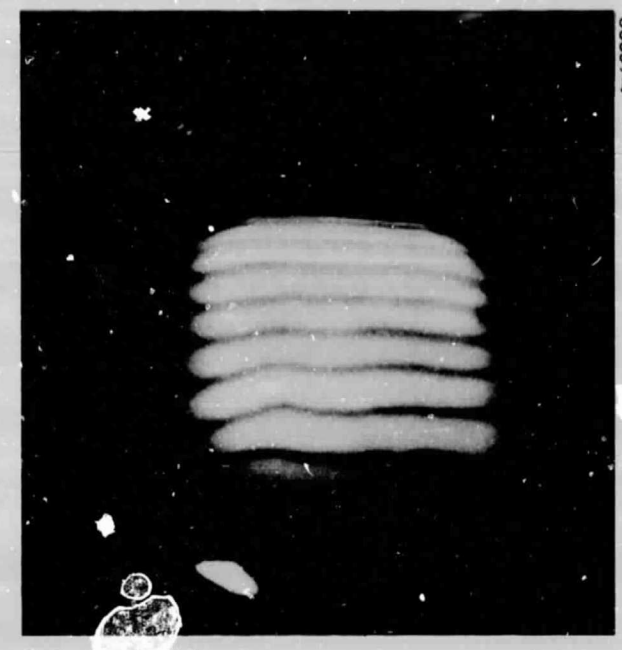

FIGURE 4. ELEMENT 1-LARGE ALUMINUM POINTING MIRROR

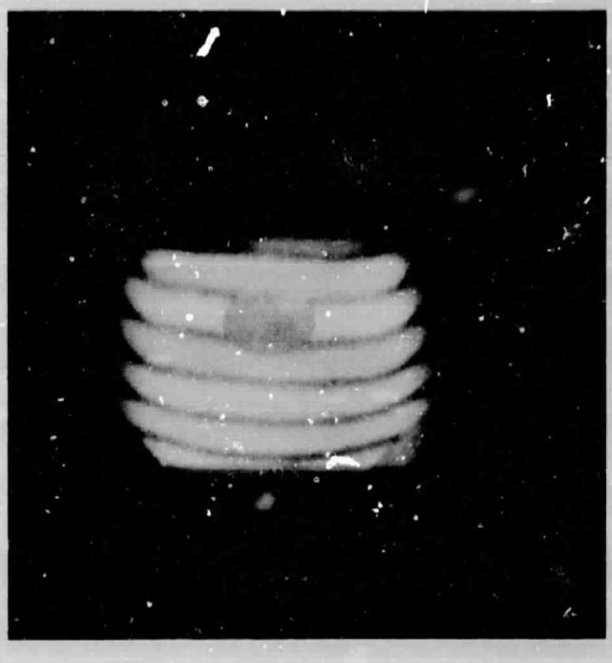

FIGURE 5. ELEMENT 2-LARGE BERYLLIUM FOLDING MIRROR

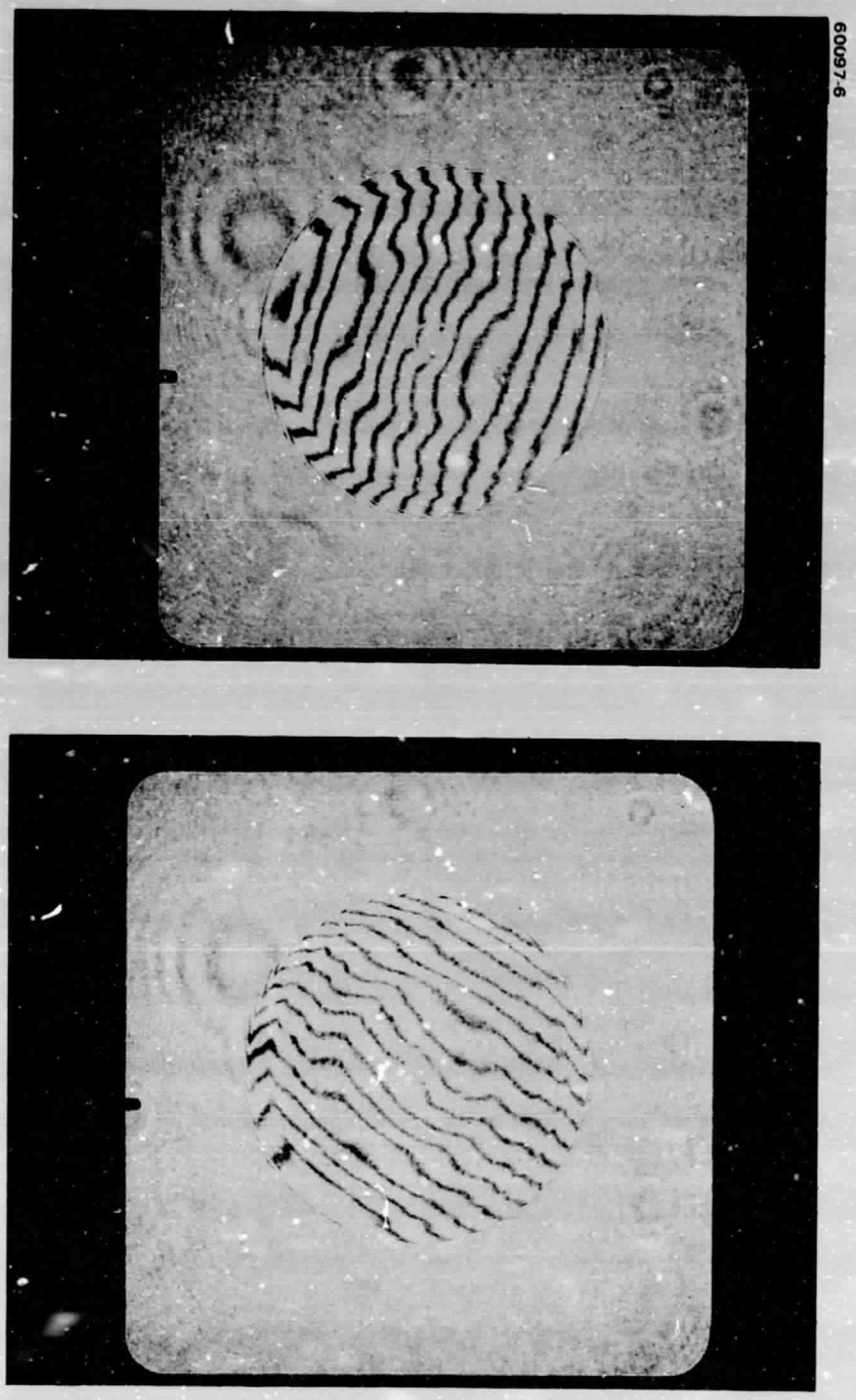

FIGURE 6. ELEMENT 3-PRIMARY MIRROR

it is hoped that the magnitude will make the problem insignificant. Further tests will be made on this mirror before installation (see below). The data for this mirror is summarized as follows:

Diameter	7.236 inches
Focal length	10.636 ± 0.001 inches
Centering	<0.005 inch
Radius of curvature (vertex)	21.272 ± 0.002 inches
Overall deviation	1-3/4 fringes
Local smoothness	<2 arcsec (95% c.a.)
Astigmatism	1 fringe
Surface finish	60/40
Back surface	Parallel to 0.001 inch

Figure 7 is the beryllium secondary mirror, element 4. There is significant rolloff near the inner and outer edges of this mirror, but it is difficult to assess the magnitude of any effects without further testing. The data for this mirror reads:

Diameter	1.377 inches
Focal length	1.500 ± 0.001 inches
Radius of curvature	3.000 ± 0.001 inches
Overall deviation	2-1/4 fringes
Centering	<0.005 inch
Smoothness	<2 arcsec (95% c.a.)
Astigmatism	1/4 fringe
Test wavelength	0.633 μm
Surface	60/40

Figure 8 is the small beryllium folding mirror (element 5). This element establishes the obscuration ratio for the system, and the edges of the center hole must be as sharp as possible. It is evident that the efforts expended to maintain good edge quality were successful, as no rolloff can be seen. The 1 mm allowance for this effect is clearly conservative, and the true obscuration ratio of the system should be less than originally planned.

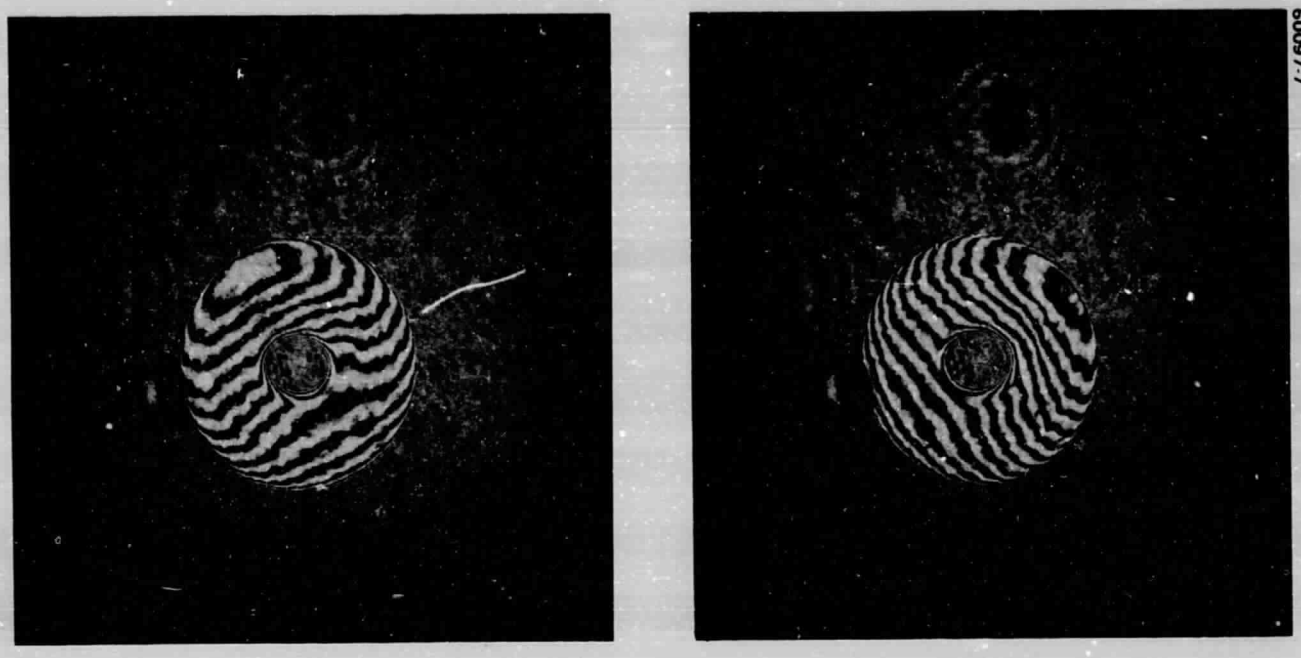

FIGURE 7. ELEMENT 4-PARABOLOIDAL SECONDARY MIRROR

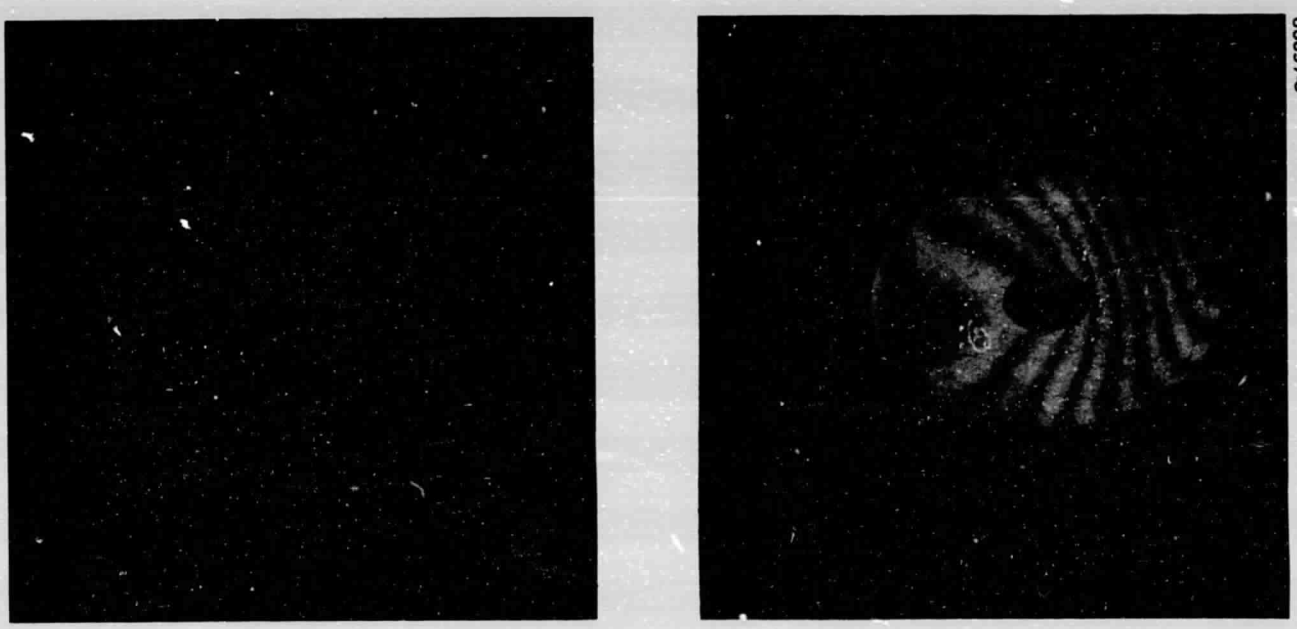

FIGURE 8. ELEMENT 5-SMALL BERYLLIUM FOLDING FLAT

The data sheet for element 5 shows a deviation of 2 fringes concave, astigmatism of 1/2 fringe, and a surface finish of 60/40. Test wavelength was 0.589 μm.

Figure 9 shows the small aluminum folding elements 6 to 9. All pieces are within 1-3/4 fringes overall, show less than 2 arcsec smoothness, astigmatism of 3/8 fringe or less, and surface quality better than 80/50. Test wavelength was 0.589 μm.

Two reflectance curves were received, one at normal incidence and a second at 45°. Both runs were made through the visible and near IR region from 0.4 to 2.0 μm and in the vicinity of 10.6 μm. Reflectance at 10.6 μm is better than 98 percent for either angle. From 2 to 14 μm the normal incidence curve closely matches the reflectance of an evaporated gold witness sample, and from 0.4 to 2.0 μm both normal and 45° incidence curves exceed an evaporated aluminum reference. At 45°, the coating shows a pronounced reflectance dip (to approximately 83 percent) near 8 μm, apparently caused by interference in the protective coating. The heating effects of this dip in direct sunlight have not been calculated yet, but the narrow spectral region involved and the relatively low energy content of this wavelength indicate that the effect should be insignificant. Figure 10 shows the reflectance in the visible while Figure 11 shows the region near 10 μm for both normal and 45° incidence.

The optics as received are well within specification and should perform to the diffraction limit at 10.6 μm without difficulty. However, in view of the problems encountered with the receiver subsystem optics (see Section 4) additional tests will be performed before installation. These tests will consist of far field patterns for each element individually, and for elements 3 and 4 combined. The results of these tests should provide a high degree of confidence in final performance.

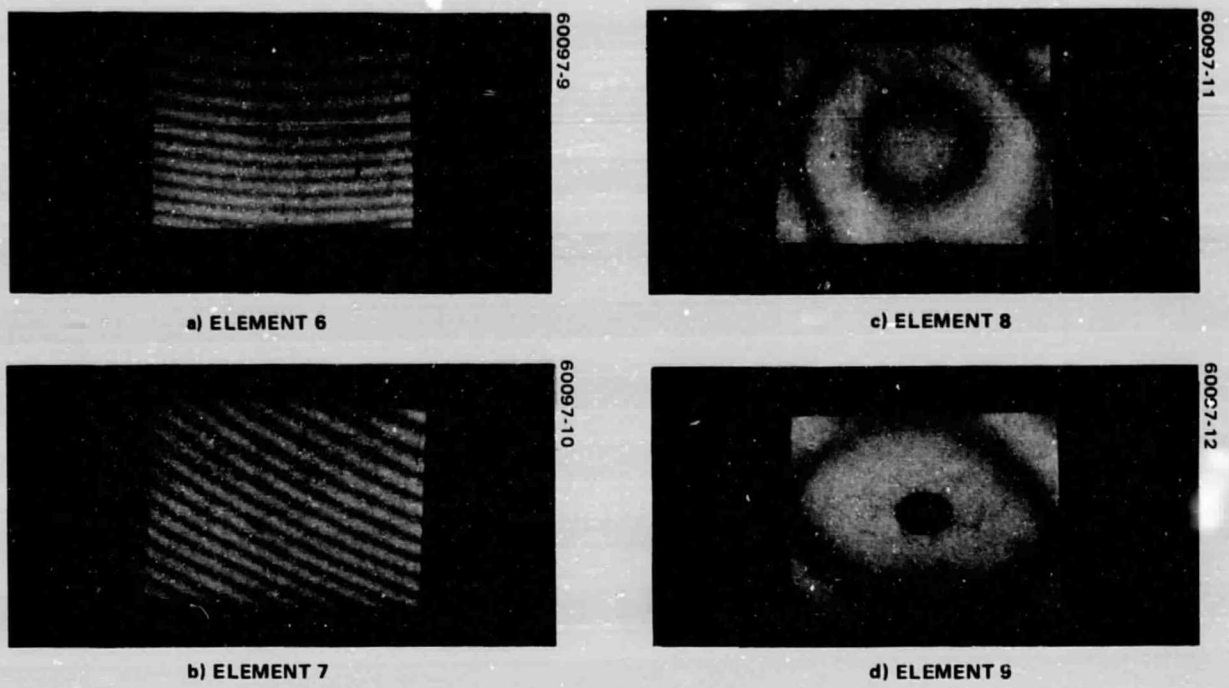

FIGURE 9. SMALL ALUMINUM FOLDING ELEMENTS

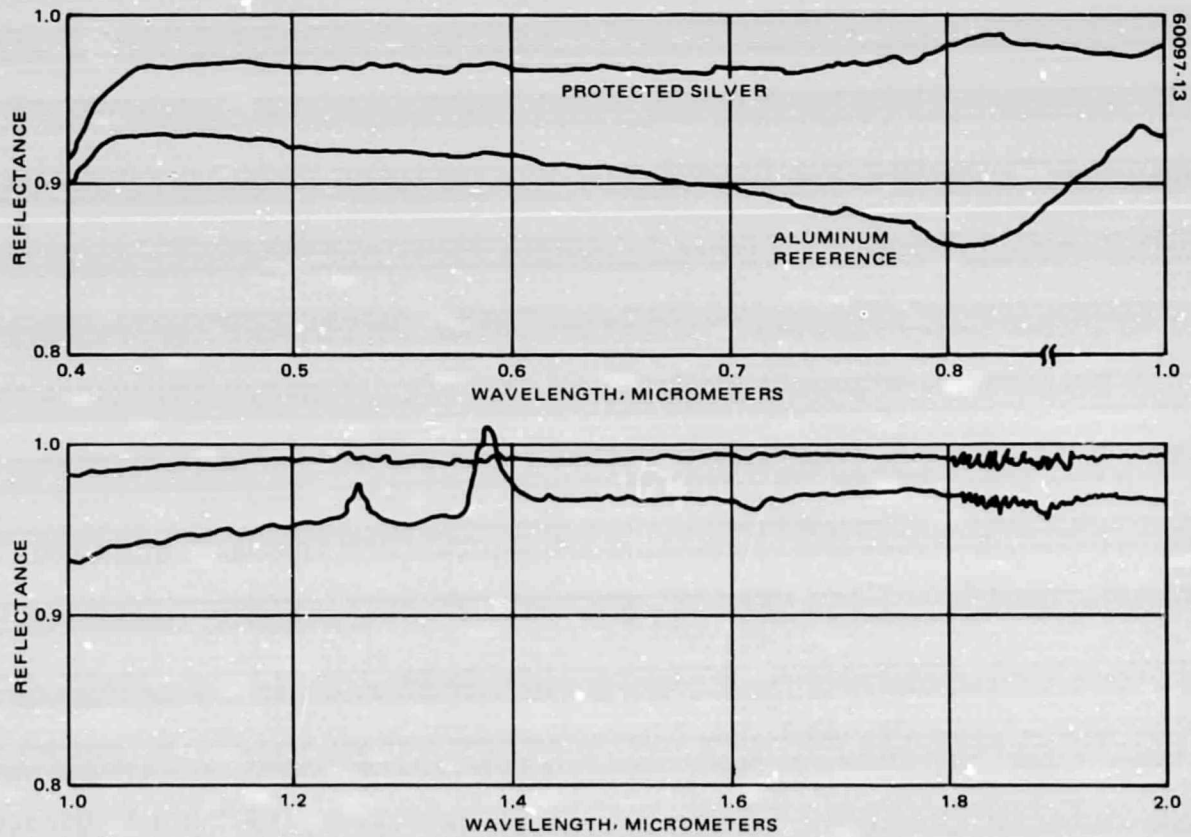

FIGURE 10. REFLECTANCE OF WITNESS SAMPLE IN VISIBLE AND NEAR-IR

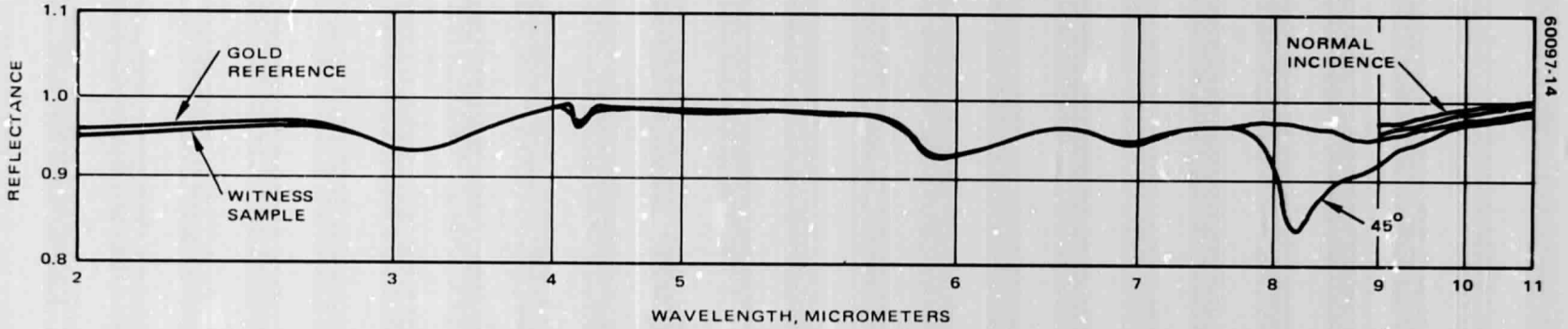

FIGURE 11. REFLECTANCE OF WITNESS SAMPLE FROM 2 TO 11 μM

4. EXPERIMENT MEASUREMENT OF OPTOMECHANICAL SUBSYSTEM OF 10.6 μm RECEIVER

SUMMARY

Last month's report indicated receiver optical performance that was less than ideal. During this reporting period an intensive effort was expended to determine the cause of this inadequacy. The entire receiver optical train was disassembled and each element checked. Combinations of elements were also checked. Finally, the receiver was reassembled and aligned with performance checks after each step.

System degradation took the form of severe astigmatism or coma in conjunction with a multilobed beam pattern. Since all measurements were made using visible light, correction factors were developed to correlate performance to that expected at the design wavelength. Under these restraints, the largest lobe of the pattern approximated the 10.6 μm Airy disc, but the comatic tails and secondary lobes fell well outside this region.

Removal of the mirrors and individual checks of the primary and secondary mirrors revealed that these elements were capable of adequate performance either individually or as a combination. Each element showed some astigmatism as well as cylindrical distortion, but all of the visible energy was contained within the 10.6 μm Airy pattern. The primary mirror is, as expected, very critical toward angular misalignment. The primary and secondary mirrors were reinstalled in the receiver with two flat elements (the large gimbal mirror and the smaller folding mirror) and rechecked. With careful alignment it was possible to partially cancel the cylindrical distortion, and satisfactory performance was achieved. Evidently part of the problem was caused by misalignment between the primary and secondary mirrors.

Attention was then turned to the remaining flat optics consisting of the two image motion compensator (IMC) mirrors and the combining mirror, all three of which are mounted on the optical bridge. The combining mirror was checked using an interferometer. Slight quadratic (spherical) distortion was noted, probably caused by the mounting technique. The curvature showed some asymmetry (astigmatism), but a check showed that the far field pattern was well within the 10.6 μm performance requirements.

The two IMC elements were not removed from the bridge, due to the alignment requirements, but were checked together. An attempt to make an interferometric check was marginally successful, but the distortion in these two elements is so severe that an accurate fringe count was impossible. A check of the far field pattern revealed the severe nature of the problem. The pattern is a multilobed array arranged in two lines at an angle of about 45^{o} with a less intense line of lobes bisecting this angle. The pattern was well outside the 10.6 μm Airy boundary. The distortion was localized to a region of the mirrors where there is an abrupt change in thickness, implying that the mirror material was stressed during manufacture and has relaxed as a function of time.

DETAILS OF OPTICAL PERFORMANCE ANALYSIS

During the previous quarter (fifth) the receiver was used in conjunction with an FM transmitter and 0.9 μm tracking system for measurements over a 7 mile range. Tracking performance of the system during these tests was unpredictable with the system breaking lock intermittently and reacquiring at a different angle. After long experience with the system and a rudimentary attempt at plotting the receiver antenna pattern, it became evident that there were three positions where the signal peaked: two closely spaced strong signals and a more remotely located secondary peak. At the time there was no way to determine whether the cause of this anomaly was atmospheric phenomena, multipath interference, or optical (antenna) imperfections.

Upon return to the laboratory, measurements were begun to isolate the cause of the problem. To provide a measure of the receiver antenna pattern, the system depicted in Figure 12 was constructed. The reversals in a triangle wave are counted, converted to analog voltages, and the resulting stairstep together with the triangle used to drive the IMCs in a raster scan pattern. The detected signal from the receiver AGC is added to the stairstep to provide a vertical scope display. The horizontal drive is controlled by the triangle wave, with a small amount of stairstep added to provide a slewing effect. The result is a scope pattern that can be viewed as a three dimensional representation of the signal amplitude as a function of receiver pointing angle.

Using the above display device, plots were made of the heterodyne signal amplitude pattern, the results of which are shown in Figure 13. The three lobed performance that was suspected was confirmed, with one isolated lobe and a pair of lobes that appear to be a large single lobe with an interference fringe through it. The vertical deflection was derived from the AIL receiver AGC signal and is very nonlinear; quantitative interpretation is not valid as would be suspected from the flat tops on the lobes. The angular distance between the two pictures is nearly $1/2^{o}$. The angular coverage of each picture is listed in the figure; the single lobe is considerably smaller than the double lobe.

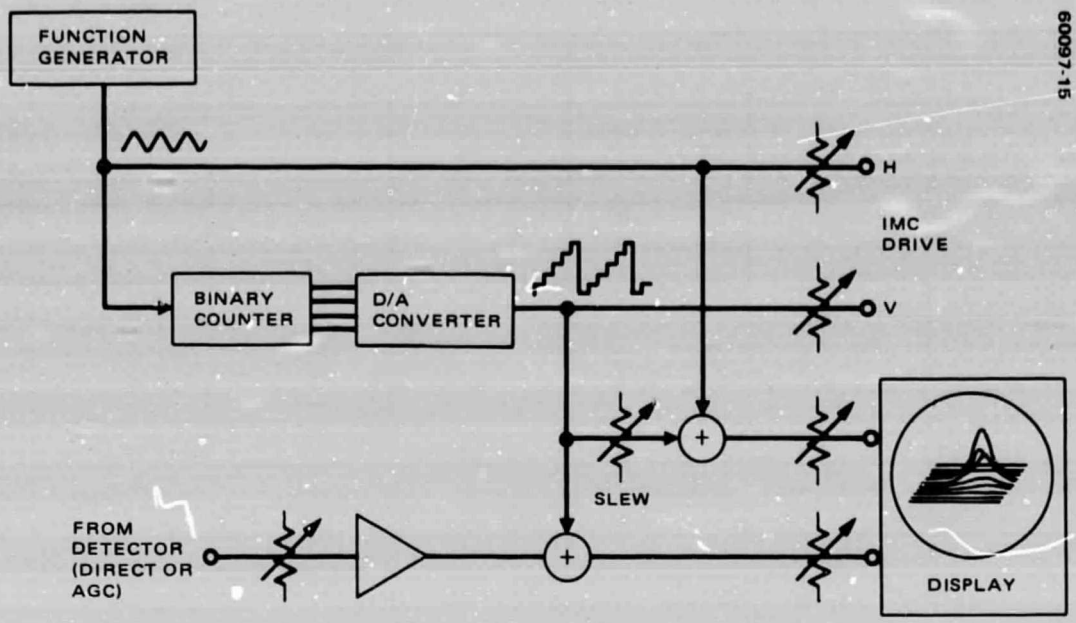

FIGURE 12. ANTENNA PATTERN DISPLAY

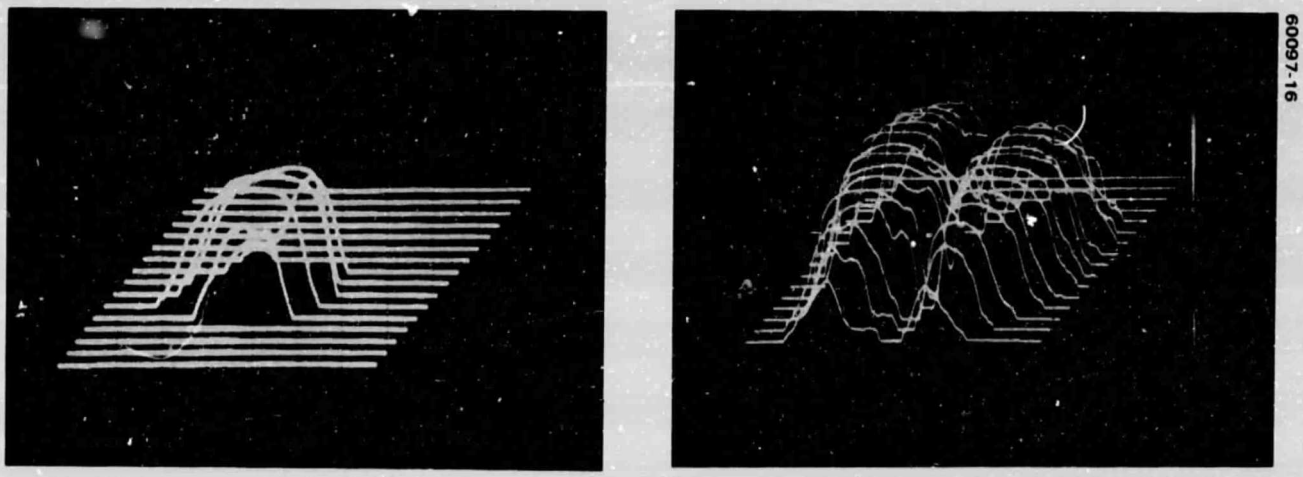

• ANGULAR COVERAGE OF RASTER IS 1.04 mr HORIZONTAL X 0.91 mr VERTICAL

• ANGULAR COVERAGE OF RASTER IS 3.9 mr HORIZONTAL X 2.1 mr VERTICAL

FIGURE 13. ANTENNA PATTERN DURING 7 MILE TESTS (PICTURES WERE SEPARATED BY 8 5 MR)

Optical tests of the receiver were then conducted using a HeNe laser source in conjunction with a 20-inch collimator as diagrammed in Figure 14. A portion of the 20-inch collimated beam is focused by the receiver to the plane of the detector. Projection optics are used to magnify the image and display it on a screen; the magnification of the projection optics is S_1/S_2 where S_1 and S_2 are the distances from the two focal planes to the principal planes of the projection optics. In practice a 1-inch f/1 projection lens was used at high magnifications (>50) so the magnification is approximately equal to S_1.

Unfortunately, the pattern for the entire receiver was not recorded as a satisfactory technique had not been developed at this early date. The first pattern that was recorded is shown in Figure 15, which is for the primary mirror only. A two lobed pattern with severe coma is shown. The entire receiver was very similar but there were two additional tails caused by the IMC mirrors.

To determine the causes of this distortion, the receiver was disassembled and the optics were tested individually, using a technique similar to that shown in Figure 14. Thus, in the case of the primary, the mirror was illuminated by the collimator and the focal plane was projected. For the elliptical secondary, an auxiliary lens was used to form a point source at one of the two foci and the image formed at the second focus was projected. For flat optics, the reflected beam was focused by an auxiliary lens and the image projected. Small flat mirrors were also tested by use of a Michelson interferometer.

The results of these tests are shown in Figure 16 through 22. Most of these photographs were taken on 10 x 10 graph paper; thus a rudimentary calibration is possible. To this end, the magnification, f number, and computed Airy pattern diameter to the first null are shown below each photo. The Airy pattern diameter is found by:

$$D = 2.44\ f/\#\ \lambda M$$

where $\lambda = 10.6\ \mu m$ and M is the effective magnification. Values are converted to inches since the screen is 0.1 inch square. Several photos show a small circle; this is drawn to equal D.

Figure 16 shows the pattern obtained from the two test lenses used in the other setups. For this photo, the listed Airy diameter is that expected for 0.63 μm. The results clearly show that the tests were not limited by the test lenses.

Figure 17 is the pattern from the primary mirror after careful alignment to obtain a symmetrical pattern. Most of the energy falls within the 0.7-inch Airy diameter, but there is "ghosting" around the pattern. The comatic tails evident in Figure 15 are still there but are more nearly symmetric and lower in amplitude.

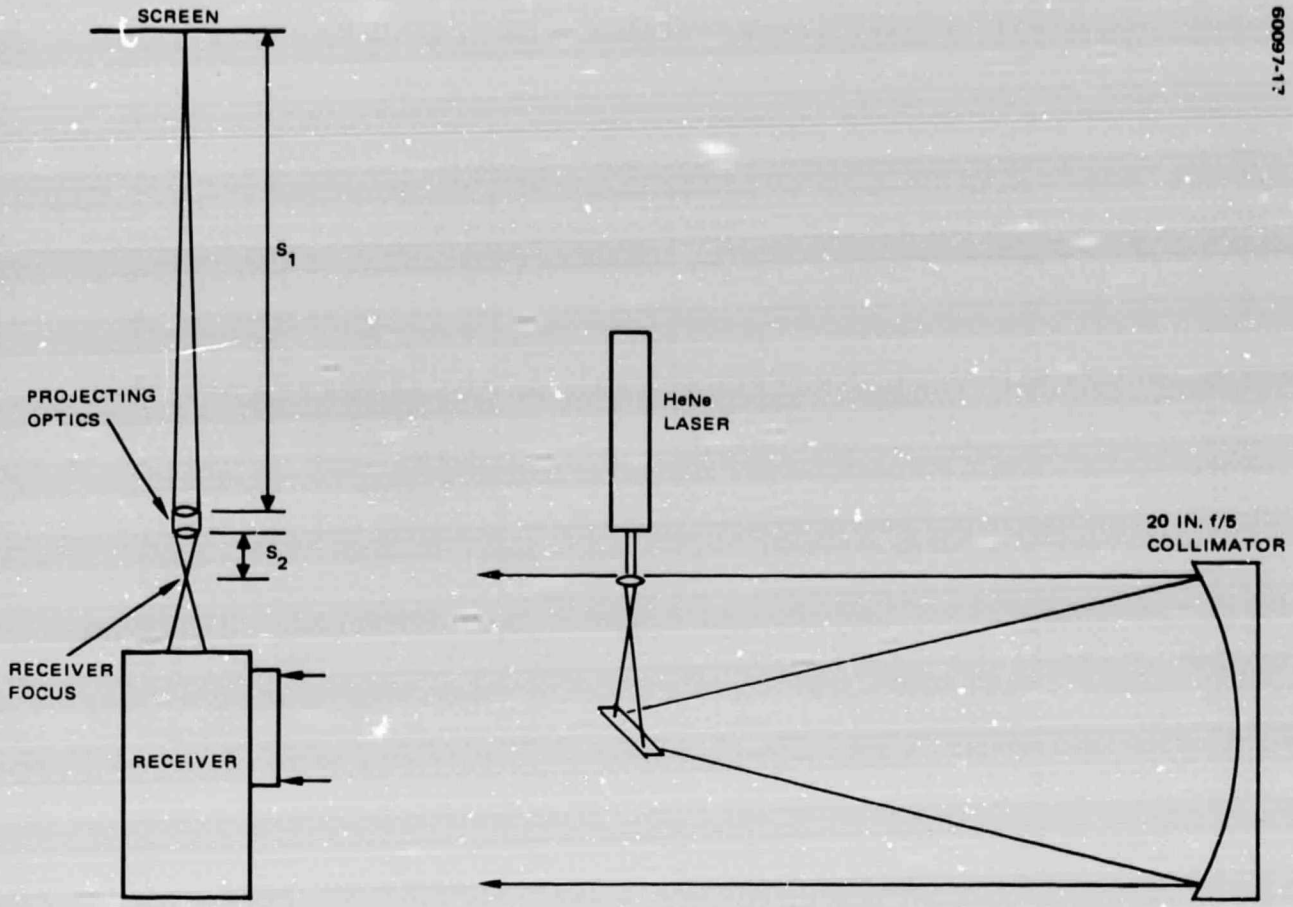

FIGURE 14. TEST ARRANGEMENT FOR OPTICS EVALUATION

FIGURE 15. FAR FIELD PATTERN; OF PRIMARY MIRROR BEFORE REALIGNMENT (NO CALIBRATION)

60097-19

TEST CONDITIONS

- f/8
- M = 280
- AIRY DIAMETER = 0.101 in. AT 0.63 μm

FIGURE 16. REFERENCE OPTICS CONSISTING OF TWO TEST LENSES

60097-20

TEST CONDITIONS

- f/2.2
- M = 314
- AIRY DIAMETER = 0.70 in.

FIGURE 17. PRIMARY MIRROR PATTERN

60097-21

TEST CONDITIONS

- f/8
- M = 260
- AIRY DIAMETER = 2.12 in.

FIGURE 18. SECONDARY MIRROR PATTERN

a) SLANT EXPOSURE TIME

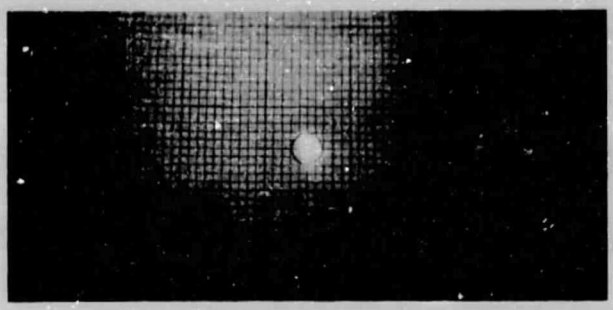

b) LONGER EXPOSURE WITH AIRY CIRCLE ADDED

60097-22

TEST CONDITIONS

- f/8
- M = 45
- AIRY DIAMETER = 0.37 in.

FIGURE 19. PATTERN FOR PRIMARY, SECONDARY, AND TWO FOLDING MIRRORS

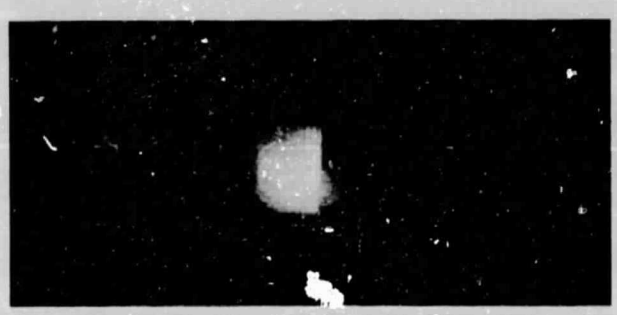

a) INTERFERENCE PATTERN SHOWING CURVATURE AND SLIGHT ASTIGMATISM

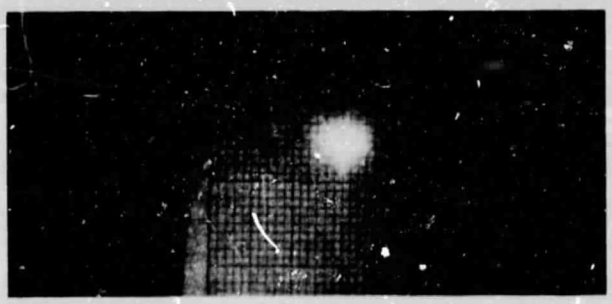

b) FAR FIELD PATTERN

60097-23

TEST CONDITIONS

- f/8
- M = 96
- AIRY DIAMETER = 1.67 in.

FIGURE 20. LOCAL OSCILLATOR COMBINING MIRROR PATTERN

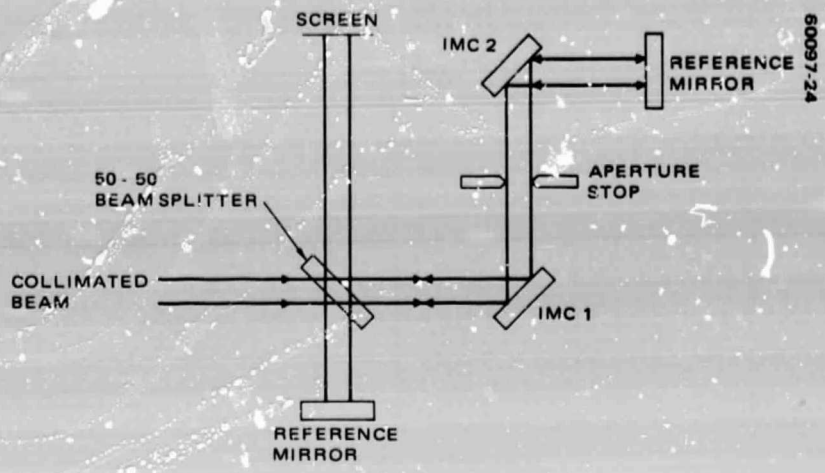

DOUBLE PASS INTERFEROMETER TEST SETUP

60097-25

- PATTERN SHOULD BE ROUND
- DISTORTION CAUSED BY SEVERE MIRROR DISTORTION

FIGURE 21. INTERFERENCE PATTERN FOR TWO IMC MIRRORS

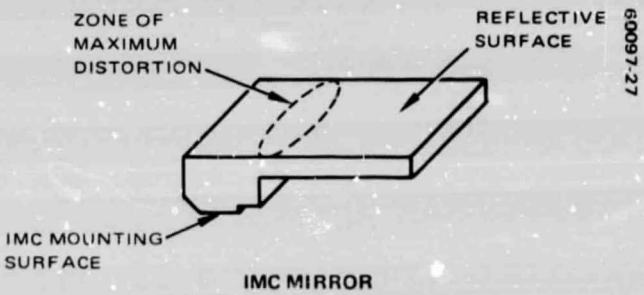

IMC MIRROR

60097-26

- PHOTO WAS NOT CALIBRATED, BUT AIRY DIAMETER IS SLIGHTLY LARGER THAN "HEAD" OF "DRAGONFLY"

FIGURE 22. FAR FIELD PATTERN OF TWO IMC MIRRORS

Figure 18 is the pattern for the elliptical secondary illuminated at its primary focus by a point source. Here nearly all of the energy falls within the 2.12-inch Airy diameter, and in fact a visible diffraction pattern (Airy = 0.13 inch) has almost formed. Again, there is significant ghosting or scattered energy.

Both the primary and secondary mirrors show some astigmatism, so an attempt was made to align the two mirrors for cancellation as the mirrors were reinstalled into the housing. Figure 19 shows the results of careful alignment of the first four elements of the optical train consisting of the gimbal mounted pointing mirror, primary, secondary, and small folding mirror following the secondary. Figure 19a shows the pattern in sharp focus, while Figure 19b was taken with a longer exposure to illuminate the screen. The circle in Figure 19b approximates the 10.6 μm Airy diameter and shows that the basic optical train of the receiver is capable of concentrating virtually all of the received energy within this circle.

The excellent results obtained on the basic telescope are encouraging; the system problems are concentrated in the relatively inexpensive flat optics consisting of two IMC mirrors and the local oscillator mirror. Figure 20 shows the local oscillator combining mirror. The top photo is an interference pattern; the lower photo is a far field pattern. There is a curvature in the mirror probably caused by the epoxy mount, and there is also a slight amount of astigmatism. The far field pattern confirms the quality of this element, as all of the energy is concentrated well within the 10.6 μm Airy diameter.

Finally, the two IMC mirrors were measured. Due to the difficulty in aligning these elements, they were not removed from the optical bridge but were tested together. Figure 21 shows the method used to obtain a double pass interferometer measurement and the results of the test. The distortion in these two elements is so severe that an accurate fringe count could not be obtained. Even using a path length as short as physically possible, the far field pattern from these two elements was beginning to form, as evidenced by the distortion in Figure 21.

Figure 22 is the far field pattern of the two IMC mirrors. The distortion is clearly excessive. By using selective masking of the input beam, it was possible to localize the source of the tails extending from the largest lobe. As shown in the diagram in Figure 22, each mirror is constructed with an abrupt change in thickness to provide a lightweight mirror with a reinforced mounting zone. Each of the two thin tails in Figure 22 corresponds to a line along the step on the back of the mirror. The heavy central tail is produced by energy from both steps; it nearly disappears when either step is masked.

To summarize, the pattern was well outside the 10.6 μm Airy boundary. The distortion was localized to a region of the mirrors where there is an abrupt change in thickness. The implication is that the mirror material was stressed during manufacture and has relaxed as a function of time. To correct this problem it is necessary to remove the mirrors from the

IMCs and refigure the surfaces. This is a high risk operation which would risk the breakage of the IMC elements.

Finally, the IMCs and combining mirror were reinstalled in the receiver. Figure 23 shows the results. Figure 23a is the full aperture of the receiver, and is clearly not acceptable. In Figure 23b a mask is used that restricts the input diameter by 1/2, thereby masking out most of the distorted zones on the IMC mirrors. (Under these conditions the Airy pattern is two times the diameter of the detector.)

Figure 24 is an antenna pattern recorded after realignment. The recording was made using noncoherent detection. The central peak has a half width of about 273 μrad, about 1.8 times diffraction limited performance. The ring of energy around the central peak is difficult to explain; the form is similar to the scattered energy visible in Figure 17. The ring is not complete; the picture shows essentially all that was visible in this test. The approximate diameter of the implied circle is about 3.8 mr.

The antenna patterns taken in the heterodyne mode of operation were inconsistent and showed very little correlation to the non-heterodyne pattern. The most probable reason is improper alignment of the local oscillator. The local oscillator is introduced into the center of the converging received signal beam through a hole in a folding mirror upstream from the detector. Proper alignment requires the received signal to be centered on the mirror and focused on the detector, and the local oscillator to be centered through the hole to the detector. If these conditions are not met, the two signals will interfere improperly at the on axis position, resulting in increased sensitivity at some off-axis position. The on-axis position will suffer from wavefront tilt with drastically reduced sensitivity. The twin lobe seen in Figure 13b is one possible result of wavefront tilt. Unfortunately, there are insufficient adjustments and inadequate access to the optical train to either correct or verify these conjectures.

The only remedy for this problem is to rebuild the bridge incorporating the necessary additional degrees of freedom into the new design. The rebuilding of the bridge and rework of the IMCs will not be attempted at this time since it would interfere with development of other components (transmitters, modulator, etc.) and because it is beyond the scope of this program. It is hoped that this effort can become part of a general upgrading of the receiver package at a later date.

60097-28

TEST CONDITIONS
- f/8
- M = 90
- AIRY DIAMETER = 0.73 in.

a) FULL APERTURE

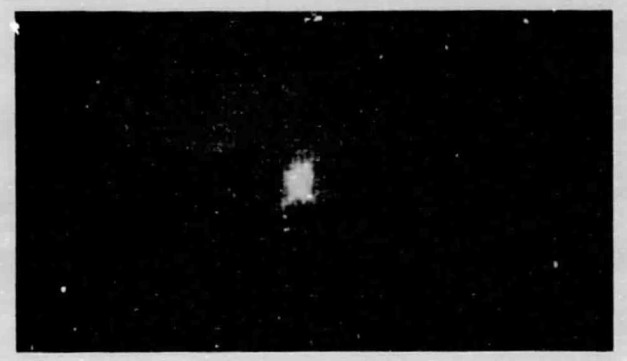

TEST CONDITIONS
- f/16
- M = 90
- AIRY DIAMETER = 1.46 in.

b) HALF APERTURE

FIGURE 23. PATTERNS THROUGH FULL SYSTEM AFTER REALIGNMENT

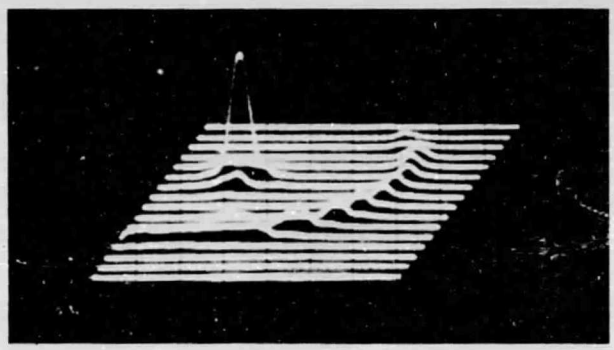

7697-29

- ANGULAR COVERAGE = 3.9 mr SQUARE

FIGURE 24. DIRECT DETECTION ANTENNA PATTERN AFTER REALIGNMENT

5. ANALYSIS TASKS

The draft material for the two link analysis volumes has been compiled and delivered to the customer for comment. No further work on this task is planned until near the end of the program when preparation of the final report is scheduled.

6. NASA CONSOLES

Two test consoles designed and built by NASA personnel have been received as Government furnished equipment to this contract for testing of the 10.6 μm receiver in conjunction with a transmitter being developed under separate contract. The console has been checked and modified to allow more extensive testing to be conducted. Input/output jacks have been added to provide the following combinations:

Direct cable connection

Simulator-receiver connection (NASA receiver)

Modulator driver-simulator-receiver

Full laser link through AIL receiver

Full laser link through NASA receiver

Operation in all modes with NRZ or Miller data

Figure 25 is a NASA photo of the two test consoles. Figure 26 is a signal path diagram for the two consoles, two relay racks, laser transmitter, and 10.6 μm receiver.

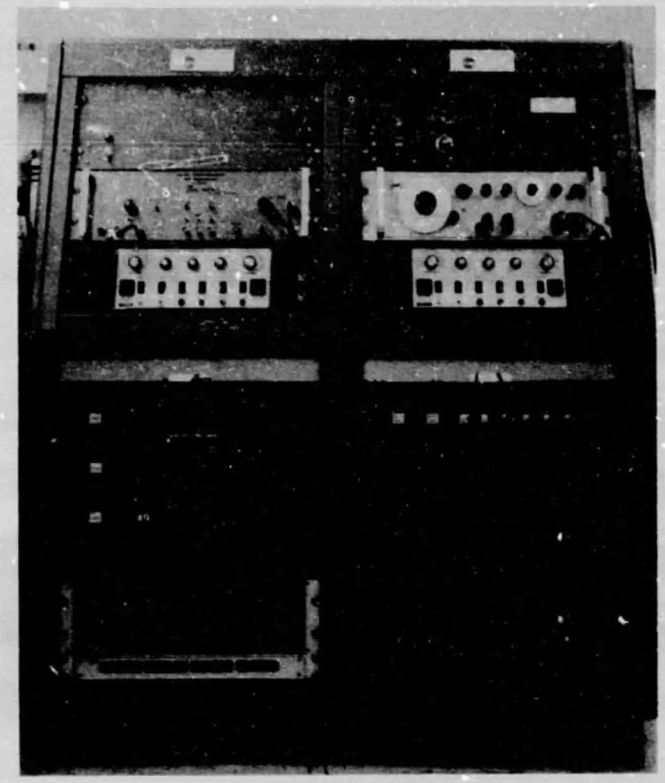

60097-30

a) TRANSMITTER

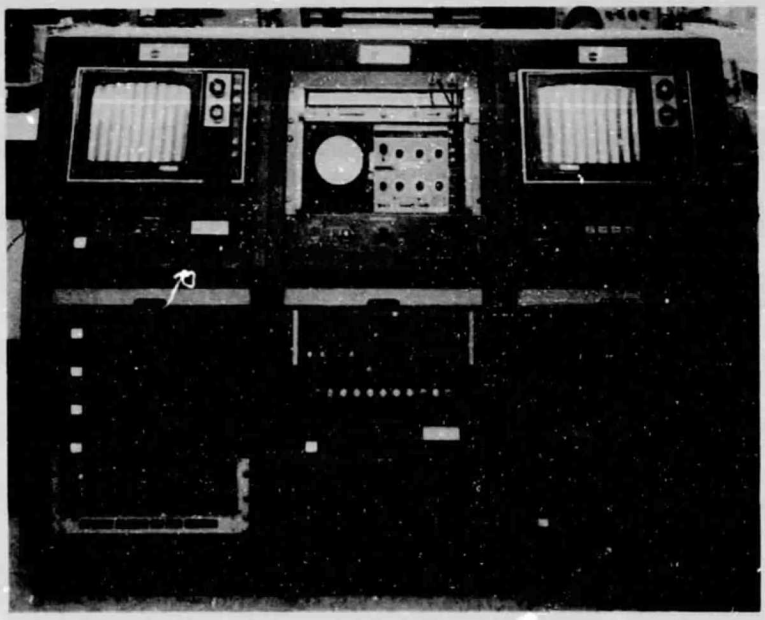

b) RECEIVER

FIGURE 25. NASA TEST CONSOLES

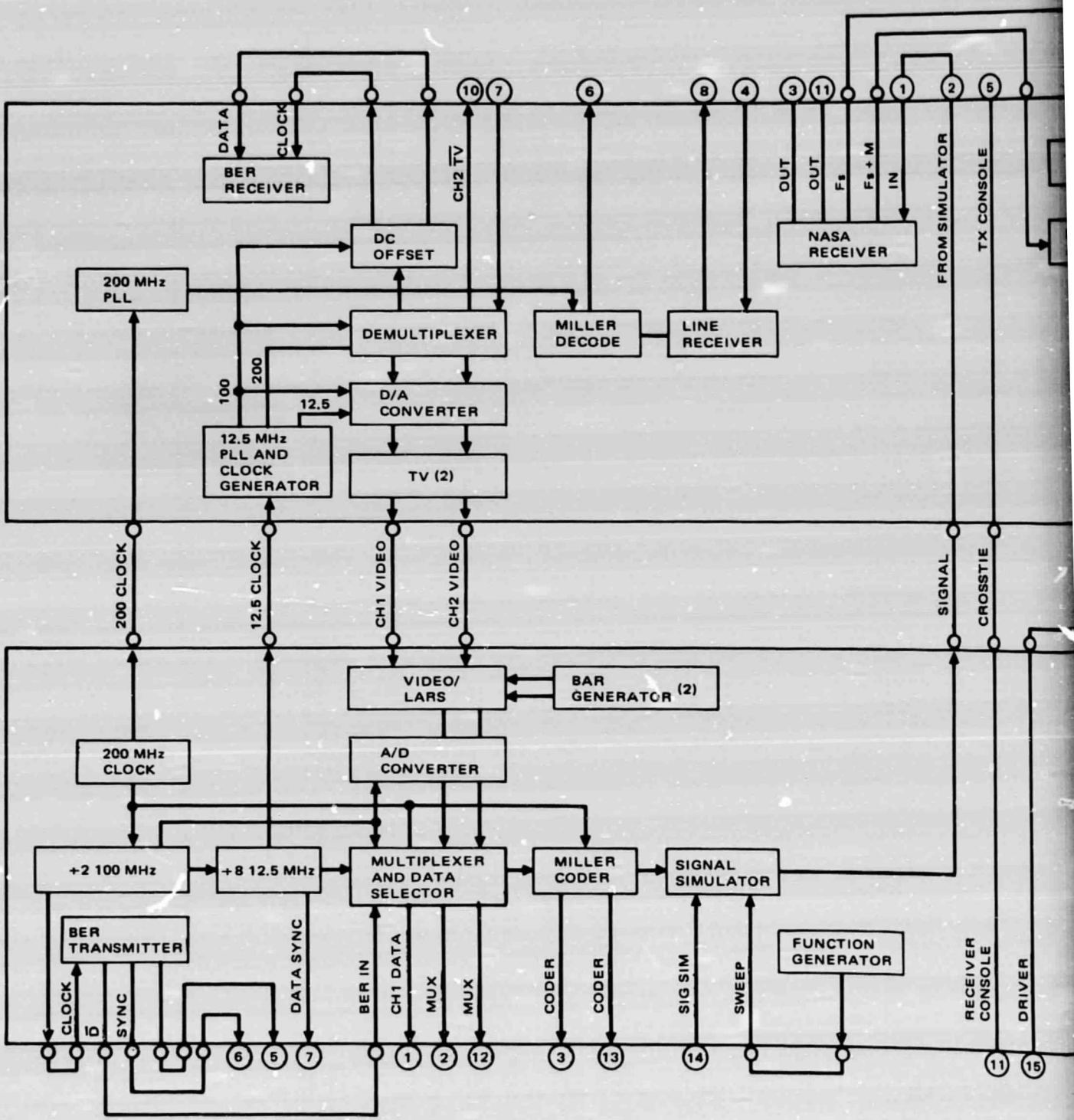

FIGURE 26. SIGNAL PATH INTERCONNECTIONS

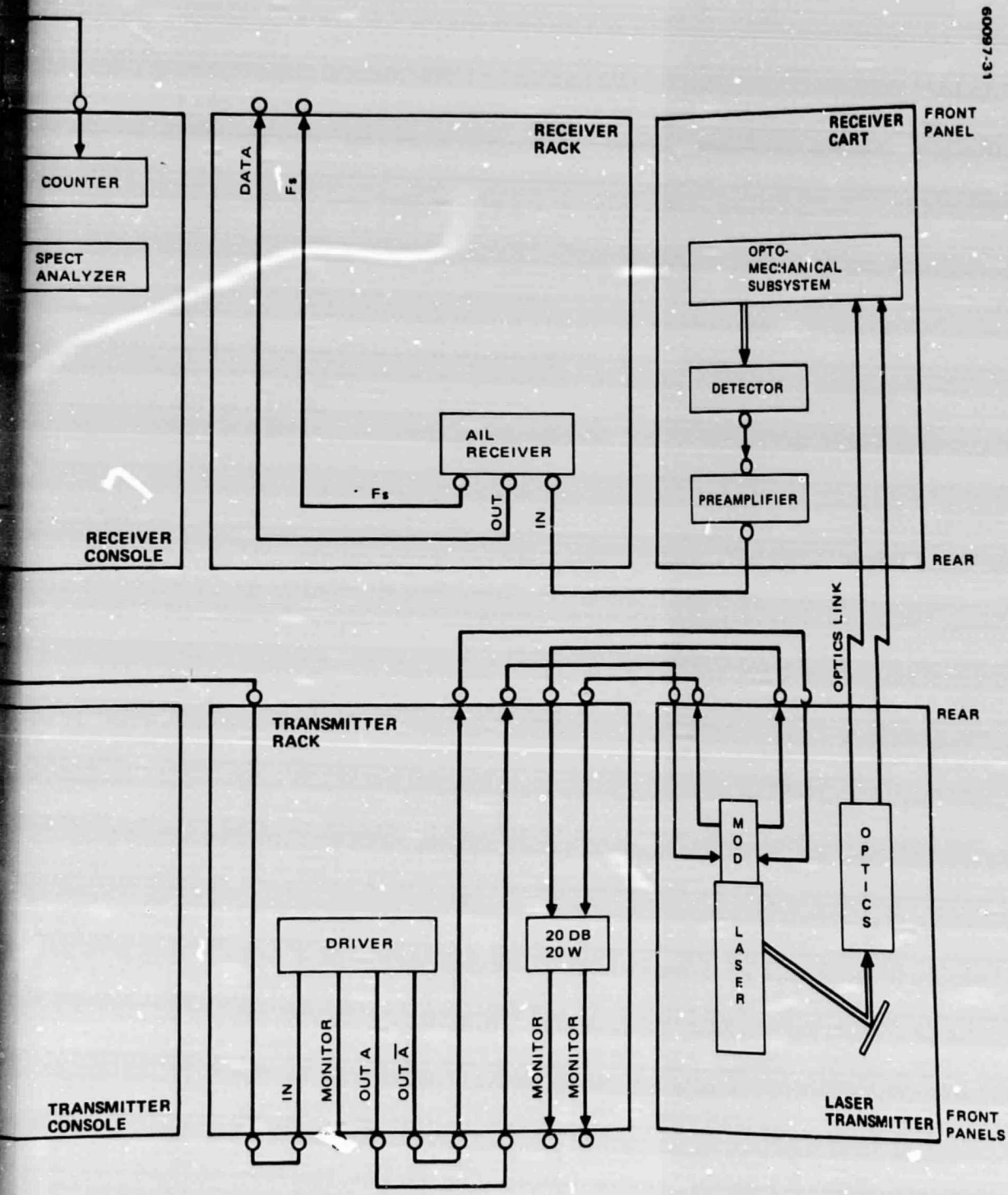
COUNTER
SPECT ANALYZER
RECEIVER CONSOLE
DATA
Fs
RECEIVER RACK
AIL RECEIVER
Fs
OUT
IN
RECEIVER CART
FRONT PANEL
OPTO-MECHANICAL SUBSYSTEM
DETECTOR
PREAMPLIFIER
REAR
OPTICS LINK
REAR
TRANSMITTER RACK
DRIVER
IN
MONITOR
OUT A
OUT Ā
20 DB 20 W
MONITOR
MONITOR
MOD
LASER
OPTICS
TRANSMITTER CONSOLE
LASER TRANSMITTER
FRONT PANELS

60067-31